www.cadanda.com
Computer-Aided Design AND APPLICATIONS

Designing Natural-Tooth-Shaped Dental Implants based on Soft-Kill Option Optimization

Yongki Yoon[1], Xiaoyan Sun[2], Jen-Kuang Huang[3], Gene Hou[4], Krzysztof Rechowicz[5], Frederic D. McKenzie[6]

[1]Old Dominion University, yyoon@odu.edu
[2]Old Dominion University, xsunx003@odu.edu
[3]Old Dominion University, jhuang@odu.edu
[4]Old Dominion University, ghou@odu.edu
[5]Old Dominion University, krech001@odu.edu
[6]Old Dominion University, rdmckenz@odu.edu

ABSTRACT

This paper presents the refinement and optimization of three-dimensional (3D) dental implants with the complex root shapes of natural teeth. These root shapes are too complex to be drilled manually like current commercial implants and so are designed to be conducive to robotic drilling utilizing milling algorithms. Due to the existence of sharp curvatures and undercuts, anatomically correct models must be refined for 3D robotic milling and these refined shapes must be shown to be optimized for load bearing. Refinement of the anatomically-correct natural tooth-shaped models for robotic milling was accomplished using Computer-Aided-Design (CAD) tools for smoothing the sharp curvatures and undercuts. The load bearing optimization algorithm is based on the Soft-Kill Option (SKO) method, and the geometries are represented using non-uniform rational B-spline (NURBS) curves and surfaces. Based on these methods, we present optimized single and double root-shaped dental implants for use with robotic site preparation.

Keywords: mesh**,** dental implants, finite element analysis, shape optimization.
DOI: 10.3722/cadaps.2013.59-72

1 INTRODUCTION

Advancements of computing schemes for biological analysis and computer-aided design (CAD) have led to rapid development in biomechanical applications ranging from biotechnology to tissue engineering [1]. Based on the designed CAD geometrical configuration, finite element analysis (FEA) in dental research has been significantly used for several decades to reduce time and cost [2-7], and to provide specific quantitative information at any location within geometrical model. Thus FEA has become a highly required analytical tool for assessment in dentistry. We utilize a combination of CAD

analysis and FEA optimization to design natural root shapes including a two-root shape for dental implants that is intended for automated robotic site preparation [8] and subsequent manual implantation. These novel shapes are intended to provide a significant increase in the stability of implants which we believe will increase the long term (> 5 years) success rate of dental implants.

There are only two types of implants in use today. Research on traditional implant designs and their finite element analyses (FEA) include variations on the thread helix of a screw and screw bore [9] [10] as these screw types of implants are overwhelmingly used commercially. Another type of implant is called **ò**press fit**ó** which does not have a helix but retains the shape of a screw and is utilized much less frequently in a clinical setting because of its poor initial stability. Both these implants suffer from potential instability in large molar regions, thereby having a **ò**lollipop effect**ó** i.e. large disc on small stem. This inherent instability significantly affects the long term success. In this paper, we address the long term stability of implants especially for large molar teeth by designing implants that mimic the better stability of natural teeth roots that are frequently double roots in the molar regions. We design a revolutionary type of single and double root implant that is based on the press-fit type of implant. These, however, are much more complex than simple screw shaped implants. Thus, sophisticated 3D models are required to better understand the mechanical behavior of the jaw bone structure and prosthetic dental restorations.

There are many papers utilizing FEA to evaluate implant designs. Fok et al. (2006) [11] provides a direct comparison of experimental and theoretical results in biomechanical studies to achieve validation. The authors utilized MD Patran 2010 [12] to model a simplified 3D mandibular segment with implants. However, no researchers evaluated 3D designs that mimicked natural root shaped implants and their viability for stability and jaw bone drilling site preparation. The potential usability of an implant must satisfy the criteria that the dental drill can attain the shape of an implant so that it may be inserted. Therefore, undercuts and sharp curvatures in a natural root form is not viable. Our hypothesis is that natural root form templates can be designed that meet the level of stability in bone that is similar to natural teeth while maintaining feasibility for site preparation. The measure of stability we utilize is the satisfactory distribution of forces along the intersection with bone.

The first step of modeling is to use CAD to define the desired bone and implant geometry. Then this is followed by defining the material behavior in terms of the Youngôs modulus and Poissonôs ratio for various mandibular bone components and the implant for FEA. After applying the load and boundary conditions, the various parameters and their contributions to the stress profile can be evaluated. Based on our FEA model, a biologically-inspired adaptive growth method called Soft-Kill Option (SKO) [13,14,15] was introduced to design the optimized implant shapes which are able to reduce the stress distribution around the interface between bone and the implant. Previously, SKO was only applied to 2D designs and we adapted the SKO method to perform in 3D topology optimization. In our method, the topology of the body and associated implant is completely defined and various parts of the body may have non-uniform local stresses based upon the impact of the implant. The objective of the optimization process is to find the best structural layout of an implant to minimize the maximum local stress. This paper validates our hypothesis by comparing our optimized implant template designs with un-optimized natural teeth to obtain desirable distribution of forces.

2 MATERIALS AND METHODS

2.1 Model Preparation

In this research, two different types of natural root-shape CAD models were prepared for the Finite Element Analysis (FEA). Our standardized set of natural-root-form implants were designed based on the 3D shape of human teeth. The 3D models of human teeth were extracted from a digital anatomically correct female skeleton. Among all the 32 teeth, the one-root part of tooth #29 and two-root part of tooth #30 were selected as the templates for FEA and further optimization since they are good representations of typical roots (Fig. 1).

After picking the templates for natural-root-form implants, shape refinement was required for the design. The shape of a natural-root is obviously much more complicated than conventional cylinder-shaped implants. Robotic operation allows precise site-preparation for the complex shapes of the natural-root-form that is not manually possible. However, due to the facts of the small scale and limited space available intra-orally, there is a need for simplification of the natural-root shapes to make automated robotic milling of the implant site a possibility.

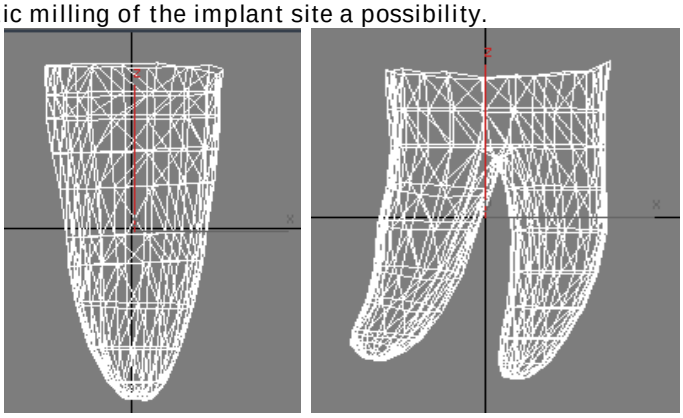

Fig. 1: Templates of natural-root shapes for FEA: (a) one-root template, (b) two-root template.

The biggest issues for natural-root-shape milling are the existence of sharp curvatures and undercuts. Therefore, two strategies were applied using Autodesk 3ds Max to get the refined shapes of the implants. First, we performed curvature smoothing since the root of a natural tooth has the tendency of curving at its apex (Fig. 2(a)). While it might provide for better anchoring for the tooth, it requires frequent direction changes and undercuts for the milling tool, which may cause heating, failure, and obstructions during site-preparation. We smoothed the curvature by creating a segmented system for each root along its central line and then adjusted the orientations of the segments or bones to make their connections smoother (Fig. 2(b)). The bones were generated according to the curvature of the original model. The conjunction between two adjacent bones lies in wherever larger curvature change occurs. We developed a simple script which reorients the position of the lower bone with respect to the upper bone, hence reducing curvature of the implant (Fig. 2(c)). Similarly, curvature soothing was also applied to the template for other implant types.

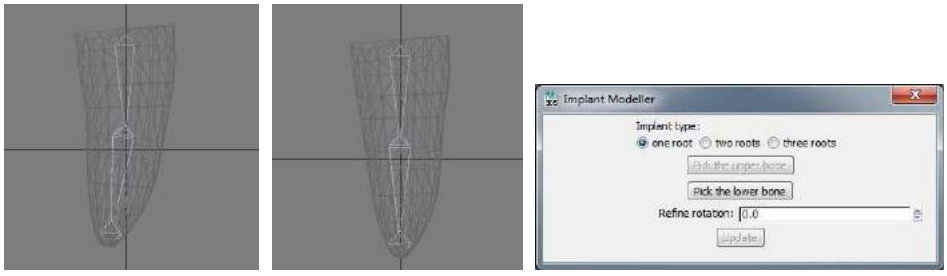

Fig. 2: Curvature smoothing: (a) initial template with bones, (b) smoothed template, (c) implant modeler windows.

When the surface of the roots was carefully inspected after the curvature smoothing, we found out there were still several undercuts in the models. Because the intraoral operation space is very small, no undercut can be manufactured in the jawbone. We applied an algorithm in Autodesk 3ds Max which accesses the position of three consecutive vertices along the centerline of the implant starting from an arbitrary point which typically is the vertex at the opening. If the position of the middle vertex is not approximately half of the distance, taking into account an arbitrary threshold, between the upper and the lower vertex, the position on the middle vertex was adjusted.

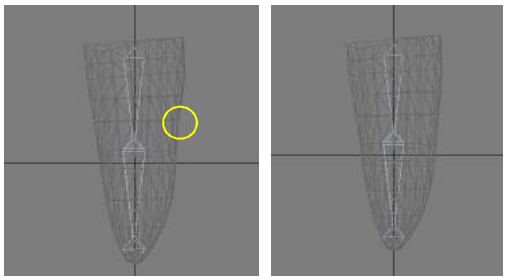

Fig. 3**:** Undercuts removal: a) model of the implant with undercuts, b) model of the implant with undercuts removed.

Since a CAD based model is initially used in this study, the boundary shape is represented by NURBS curves and surfaces to control the curvature and tangency of the model [15]. Several papers described that during the optimization process, corners in the surfaces may become sharper, which lead to increase the stresses in that region, and can face element distortion. In order to avoid the numerical errors in the meshing and Jacobian calculations, sharp edges should be smoothed. Fig. 4 shows the initial root-shape implants of an anatomically correct model without crowns (a) and (b), while models in Fig.5 represent the robotic milling refined implants from the Fig. 4.

For the finite element analysis, models of Figs. 4-5 were filled and the top surface was closed. Since original models have sharpness through the NURBS curves and surfaces, elements size was reduced by 20% and the surface was smoothed by 20% to avoid element distortion during finite element computation.

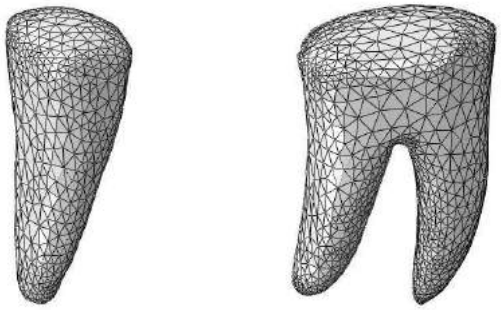

Fig. 4: Anatomically correct models: (a) one-root implant, (b) two-root implant.

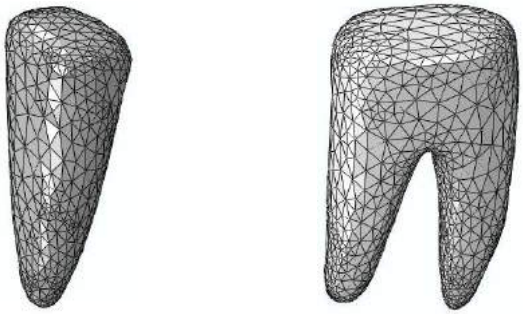

Fig. 5: Refined models: (a) one-root implant, (b) two-root implant.

2.2 Finite Element Model

Two 3D finite element models were developed using the results of the CAD refinement that represent a segment of the human mandible with four natural teeth as implants. The model was constructed from the geometry identified in the previous section and processed in Rhinoceros 3.0 and Solidworks 2010. The finite element mesh was generated in 10-node quadratic tetrahedral elements using MSC PATRAN 2010, comprising of 30,217 elements for the one root implant and 98,494 elements for the two root implant after convergence (Tab. 1). As shown in Fig. 6, the model consists of three parts: cancellous bone, cortical bone, and the natural root-shaped implants. The material properties (Tab. 2) of the implant and the bones are obtained from [14]. The interface between the cancellous and cortical bones, the implant root and the bones are assumed to be perfectly bonded. All materials used in this model are considered to be isotropic, homogeneous, and linearly elastic. Tab. 2 shows the elastic properties in terms of material types. The properties are the same in all directions, therefore, only two independent material constants of Youngís modulus and Poissonís ratio exist in an isotropic material. In Fig. 6, cancellous bone is surrounded by 1 mm thick cortical bone.

The boundary condition is applied along the bottom surface of the cortical bone and all around the sides to restrict translational and rotational movements of the structure, a load of 200 N in the vertical (z) direction was applied on the top surface of the implant, simulating a chewing force applied by the teeth from the maxillary side. The relationship between the force and angle changes with different teeth from different patients. Thus, in this paper, only a vertical force was considered to simplify the process.

Tooth Type	Elements	Nodes	Element Type
One-Root	30217	44088	C3D10
Two-Root	98494	136795	C3D10

Tab. 1: Finite element configuration for the anatomically correct models.

Materials	Youngís Modulus (GPa)	Poissonís Ratio
Cortical Bone	13.7	0.3
Cancellous Bone	1.37	0.3
Implant(titanium)	110	0.33

Tab. 2: Material properties for the anatomically correct models.

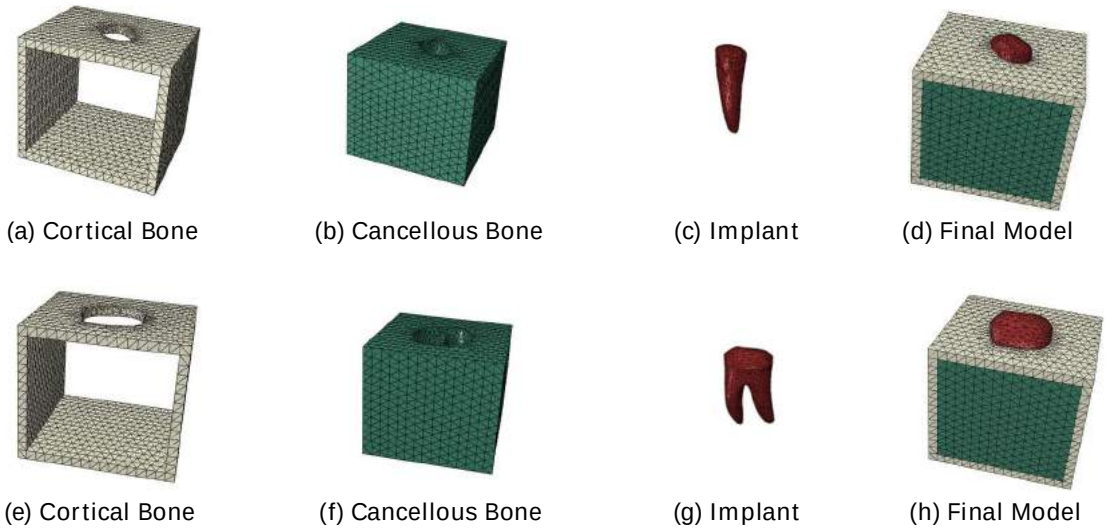

(a) Cortical Bone (b) Cancellous Bone (c) Implant (d) Final Model

(e) Cortical Bone (f) Cancellous Bone (g) Implant (h) Final Model

Fig. 6: 3D dental implants for one-root and two-root implants of an anatomically correct model.

2.3 Methodology – SKO Optimization

Topology optimization is widely used in applications where the weight of an object needs to be reduced to a minimum. The main principle in topology optimization is that the material layout should be optimized within a given design domain using a mathematical approach. The procedure of topology optimization starts with a design space that will be reduced to the final solution. The design space limits the solution and should be larger than the predicted solution. The simplest category of algorithms uses the stress to find the regions where the material is useful and where it is not. In this study, the SKO method, one of the topology optimization techniques, was used [13]. Many topology optimization methods start with a design space, which is filled with material with a certain density, 0 **Ò** ρ **Ò** 1. However, the SKO method starts with ρ=1 and then changes the material under the design

parameters and constraints. It does not keep the mass of the design constant, but it will keep the minimum stress of the design constant. The materials used for the design space in this study have the following properties: Youngís Modulus (E=1.37 GPa, 13.7 GPa), and Poissonís ratio (υ=0.3).

2.4 Overview of the Simulation

Fig. 7 illustrates the general concept of the topology optimization process. The model was created and analyzed with the following steps using FE software, ABAQUS/CAE/STANDARD [17]. Firstly, a FE model was created by Patran 2010, and then converted to an ABAQUS input file for the SKO optimization. In order to update the Youngís modulus, a user defined material subroutine (UMAT) was used to define the mechanical constitutive behavior of two different materials ð cortical and cancellous bone, while the implant has a constant material property. The UMAT subroutine updates the stresses and solution-dependent state variables at the end of the increment which can provide the material Jacobian matrix for the model. A FORTRAN environment is set up to manage the interaction between the ABAQUS input file and the UMAT subroutine.

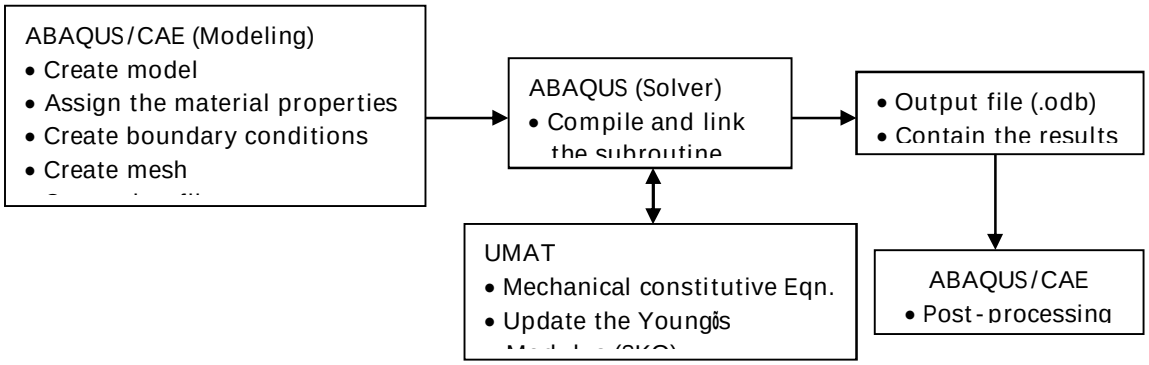

Fig. 7: Diagram of optimization process.

2.5 Three Dimensional SKO Implementation

The SKO optimizing process [13] iterates in order to find the optimal solution as illustrated in Fig. 8. The process was started with both the anatomically correct model and the model that was refined for robotic milling. The stresses are evaluated in each iterations and depending on the stress level in the elements, the elastic modulus is adjusted. Elements with high stresses are made a bit stiffer before the next iteration and vice versa. The steps are as follows:

- Start with a design space and fill it with finite elements. The user should select which material will be assigned in each iteration during computation if there are several materials;
- Generate a FEM-simulation and check the stresses in the part;
- Let each elementís material stiffness is a function of the stress in the previous iteration $E_{i+1} = f(\sigma_i)$ (Eqn. (2.5));
- Check the convergence of Youngís modulus; Step 2 and 3 should be repeated until the process converges; and then
- Optimized solution.

One can also introduce a global reference stress, σ_{ref}, for the entire model. Eqn. (2.1) was employed to update the Youngís modulus in design space.

$$E_{i+1} = E_i + k(\sigma_i - \sigma_{ref}) \tag{2.1}$$

In Eqn. (2.1), the global reference stress controls the variation of the Youngôs modulus and k is a positive scaling factor to adjust the speed of the process of updating the Youngôs modulus. In this study, three different materials were considered: implant, cortical bone, and cancellous bone. Thus, one has to limit the Youngôs modulus such as $E \in [E_{\min}, E_{\max}]$

$$i.e. \quad \begin{matrix} E_{i+1} = E_{\min} & if\ \sigma_i \le \sigma_{ref} \\ E_{i+1} = E_{\max} & otherwise \end{matrix} \tag{2.2}$$

where E_{min} denotes either cortical bone or cancellous bone, and E_{max} denotes the implant. In this way, a reasonable scaling factor, k, will be calculated as follows:

$$k = \frac{(E_{\max} - E_{\min})}{\sigma_{ref}} \tag{2.3}$$

In this research, the reference stress in Eqn. (2.1) is compared with the stress calculated in the 3D model as the von Mises stress using Eqn. (2.4) which is implemented in the UMAT subroutine.

$$\sigma_{VM} = \sqrt{\frac{(\sigma_1 - \sigma_2)^2 + (\sigma_2 - \sigma_3)^2 + (\sigma_1 - \sigma_3)^2 + 6(\sigma_{12}{}^2 + \sigma_{23}{}^2 + \sigma_{13}{}^2)}{2}} \tag{2.4}$$

It is more effective to start using a lower value for the reference stress and then increase it slowly from cycle to cycle until the process converges under the design constraints indicated in Eqn. (2.5).

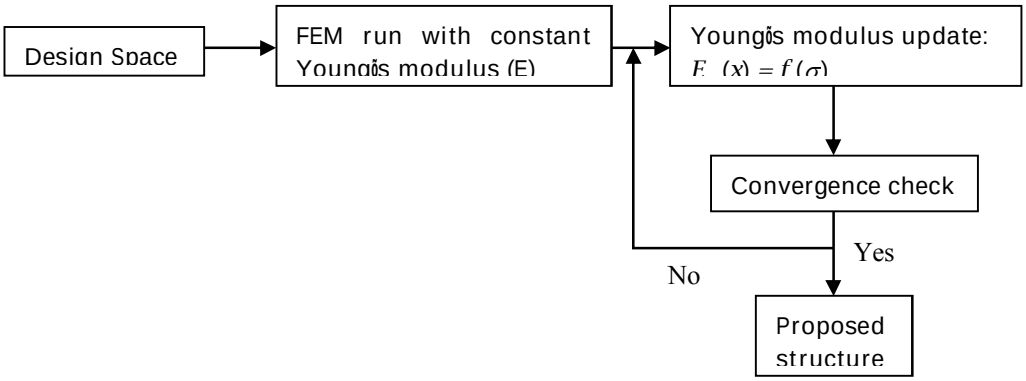

Fig. 8: Flowchart of the SKO.

$$\begin{bmatrix} \sigma_{xx} \\ \sigma_{yy} \\ \sigma_{zz} \\ \sigma_{yz} \\ \sigma_{zx} \\ \sigma_{xy} \end{bmatrix} = \frac{E}{(1+\nu)(1-2\nu)} \begin{bmatrix} 1-\nu & \nu & \nu & 0 & 0 & 0 \\ \nu & 1-\nu & \nu & 0 & 0 & 0 \\ \nu & \nu & 1-\nu & 0 & 0 & 0 \\ 0 & 0 & 0 & 1-2\nu & 0 & 0 \\ 0 & 0 & 0 & 0 & 1-2\nu & 0 \\ 0 & 0 & 0 & 0 & 0 & 1-2\nu \end{bmatrix} \begin{bmatrix} \varepsilon_{xx} \\ \varepsilon_{yy} \\ \varepsilon_{zz} \\ \varepsilon_{yz} \\ \varepsilon_{zx} \\ \varepsilon_{xy} \end{bmatrix} \tag{2.5}$$

Section 3 studies the effect of local Youngôs modulus gradation in the 3D jawbone subject to a uniform axial loading on the top surface of the implant. The modulus was graded in the z direction emanating from the contact surface between implant specimen and cortical bone into the section toward the outer traction boundaries. In the UMAT subroutine, the Youngôs modulus was varied starting at the contact surface between implant and cortical bone, but now was limited in depth such that gradation did not

extend to the outer boundaries (except for the initial run to establish a baseline). The goal was to create the optimized Youngôs modulus to reduce the magnitude of stress concentration for both the anatomically correct models and the refined models.

3 SIMULATION RESULTS

3.1 Finite Element Results

The von Mises stress distribution was used to display the stress around the cortical and cancellous bone area. Stress distribution depends on assumptions made in geometry, material properties, boundary conditions, and bone-implant interface. Contour plots of von Mises stresses, recorded at the location of implant-bone contact, under axial load of 200N are shown along the insertion depth in Figs. 9(a) through 9(d). Through the half-cut of the model, nodal paths were generated to investigate how the stress varies through these lines for the one-root and two-root implants. Fig. 9 illustrates that along the cortical and implant interface, high level of von Mises stress with a maximum stress of 19.33 MPa for one-root and 17.9 MPa for two-root implants exist near the bone around the implant neck and the magnitude of stresses then decrease along the path and the increased stresses were shown around the implant root apex regions (Figs. 9(b), 9(d), 10(b) and 10(d)) in both the initial anatomically correct case and the refined case. However, the two-root implant has less von Mises stress distribution around the root apex areas than the one-root implants.

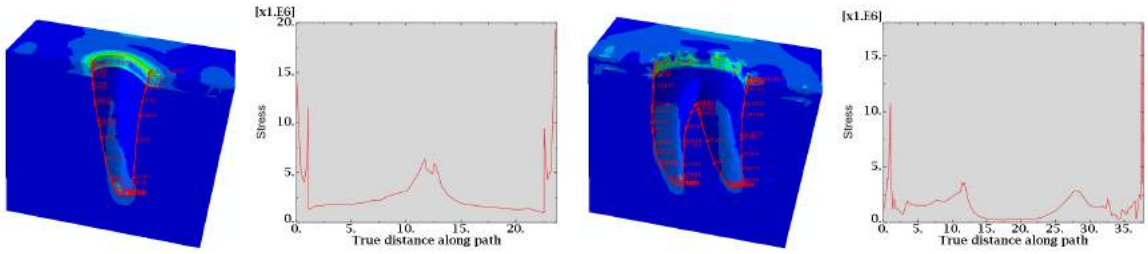

Fig. 9: Stress contours of the anatomically correct models: one-root implant - (a) contour plots with nodal path, (b) von Mises stress levels along the nodal path; two-root implant - (c) contour plots with nodal path, (d) von Mises stress levels along the nodal path.

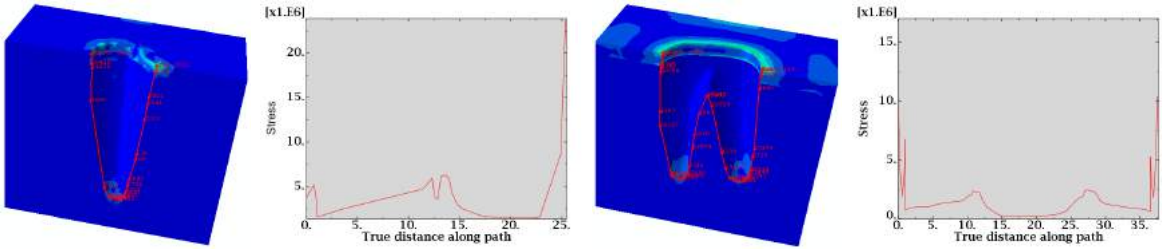

Fig. 10: Stress contours of the robotic milling refined models: one-root implant - (a) contour plots with nodal path, (b) von Mises stress levels along the nodal path; two-root implant - (c) contour plots with nodal path, (d) von Mises stress levels along the nodal path.

3.2 SKO Results – Anatomically Correct and Refined models

This section presents the results of SKO optimization of the anatomically correct and refined models. The results confirm a possibility that computer aided optimization may inspire understanding and modeling of complex natural root-shape implants. Through the optimization procedure, the geometric design space is specified, spanned with a finite element mesh and geometric boundary conditions as well as forces specified. Three Young's moduli are initially assigned to the two types of bone and the implant material of the finite elements in the design space. A structural analysis gives an initial solution to obtain a stress distribution over the domain. The stresses are combined to establish the distribution of an equivalent stress, which is the von Mises stress. The local optimality criterion used by Mattheck assumes that the stiffness of the design will globally increase when the Young's modulus is increased in regions with higher stresses and reduced where the stresses are lower. When the stresses fall below a certain threshold, the Young's modulus is replaced by the Youngís modulus of cancellous or cortical bones. This serves to modulate the shape of the implant so that the optimal shape can be determined by the optimal distribution of stresses reflected in the changing Young's modulus regions.

The SKO optimization procedure yields the results plotted in Figs. 11-14. In Fig. 11, for example, reference stresses from 2 MPa to 4 MPa were used under the axial loading of 200N to see how the material property varies for one root implant of the anatomically correct model. Note that gray and red color of the model has the same material property which is titanium. Optimized geometry adjacent to the original implant decreases progressively in thickness with increasing the reference stress. That means the circumferential stress also decreases with increasing the reference stress but its maximum value is much lower than in the initial configuration. The thickness of the optimized implant model decreases progressively but at a slow rate with increasing distance to the root. The difference between the results shown in Fig. 11 and Fig. 12 is in the choice of the reference stress used for the optimization, since different stress magnitudes exist based on the root-shapes. In Figs. 13-14, the refined model has a tendency to have more material property change in a low reference stress due probably to the wider geometric configuration than the one for the anatomically correct model.

Based on the optimized results, updated material of the top cortical bone area could be neglected since it has only 1 mm of thickness and our interest is focused near implant roots around the cancellous bone. Thus, it may be concluded that local details of the new implant shape depend on the choice of reference stress for the objective function while global features remain the same. Also results illustrate that in order to reduce the stresses around the apex of roots, root-shapes should be more rounded. Such rounded root-shapes will be introduced in section 3.3.

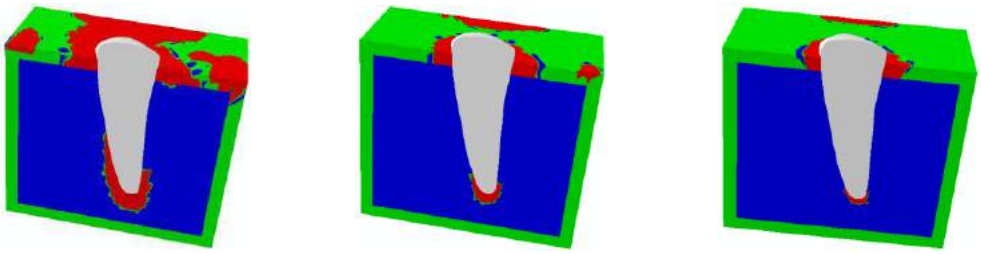

(a) σ_{ref} =2.0MPa, F=200N (b) σ_{ref} =3.0MPa, F=200N (c) σ_{ref} =4.0MPa, F=200N

Fig. 11: Optimized material property for the one-root implant of an anatomically correct model.

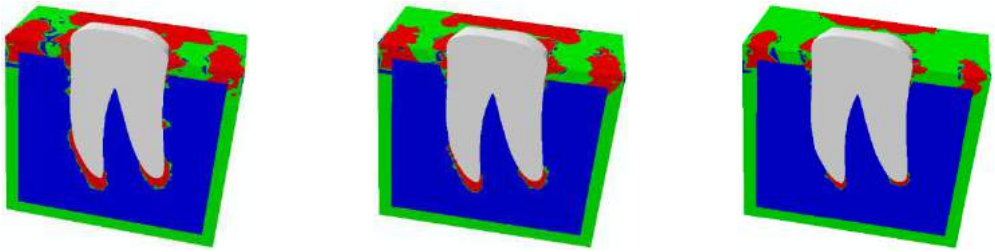

(a) σ_{ref} =1.65MPa, F=200N (b) σ_{ref} =1.8MPa, F=200N (c) σ_{ref} =2.2MPa, F=200N

Fig. 12: Optimized material property for the two-root implant of an anatomically correct model.

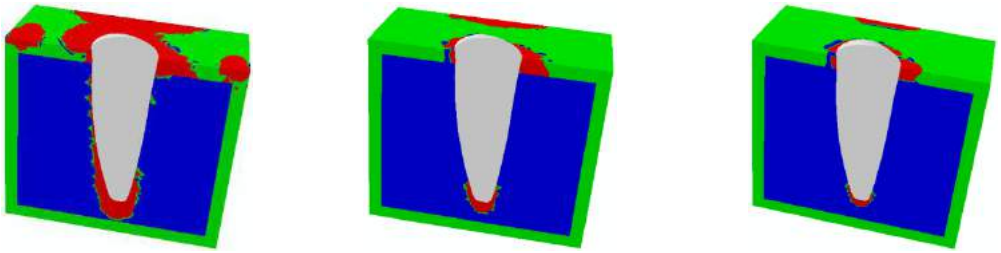

(a) σ_{ref} =2.0MPa, F=200N (b) σ_{ref} =3.0MPa, F=200N (c) σ_{ref} =4.0MPa, F=200N

Fig 13: Optimized material property for the one-root implant of a refined model.

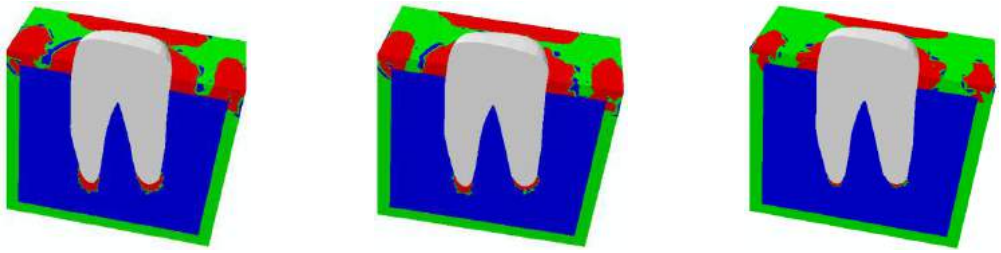

(a) σ_{ref} =1.65MPa, F=200N (b) σ_{ref} =1.8MPa, F=200N (c) σ_{ref} =2.2MPa, F=200N

Fig. 14: Optimized material property for the two-root implant of a refined model.

3.3 Optimized Implants and FEA Results

Based on SKO results, new implant shapes are created. The new optimized models without crowns have more rounded shapes around the root-tips than the previous refined models (Fig. 15c and 15d). FEM results of the optimized implants under an axial load of 200 N are shown in Fig. 16. Tab. 3 shows the stress levels for the anatomically-correct models, robotic-milling-refined models and SKO-optimized models. First, for the one-root case, the optimized model with respect to the anatomically correct model reduced the maximum stress near the implant root-tip by 21.16% from 6.38 MPa to 5.03 MPa, while it was reduced by 39.01% for two-root case. Additionally, comparing with respect to the robotic milling refined model, one-root and two-root implants have the stress reduction of 19.65% and

9.39%, respectively. Thus, the optimized implant model has significant stress decreases from both the anatomically correct model and the refined model.

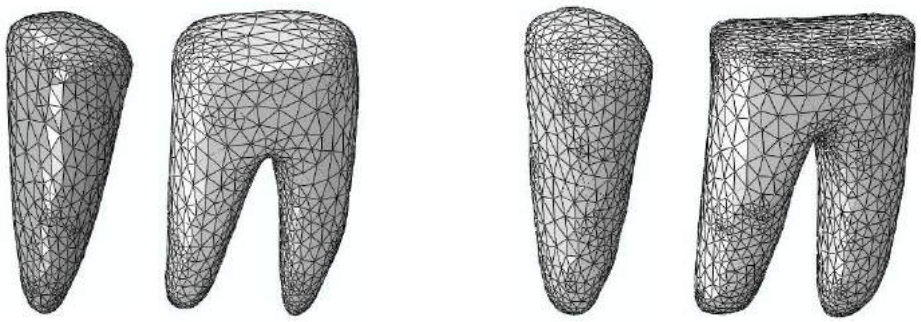

Fig. 15: Implants: refined models - (a) one-root Implant, (b) two-root implant; SKO optimized models - (c) one-root Implant, (d) two-root implant.

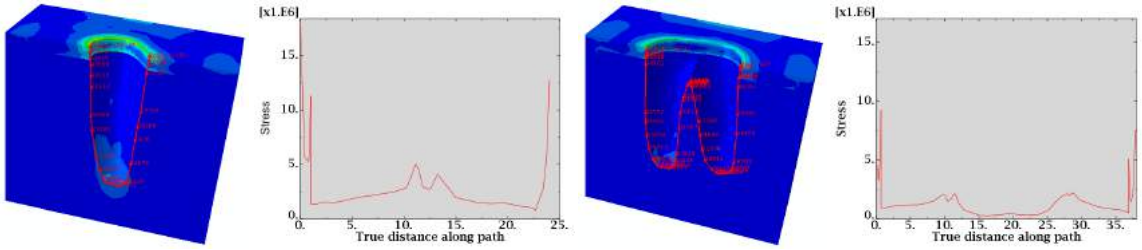

Fig. 16: Stress contours of the optimized implants; one-root implant: (a) contour plots with nodal path, (b) Von Mises stress levels along the nodal path; two-root implant: (c) contour plots with nodal path, (d) Von Mises stress levels along the nodal path.

	Anatomically Correct Model (MPa)	Robotic Milling Refined Model (MPa)	Optimized Model		
			Value	% Change from Anatomically Correct Model	% Change from Refined Model
Max. One-Root	6.38	6.26	5.03	21.16	19.65
Max. Two-Root	3.64	2.45	2.22	39.01	9.39

Tab. 3 Stress levels of three different types of models.

4 CONCLUSION

In this paper, refinement and SKO optimization techniques to design the natural root-shapes of dental implants is introduced. The anatomically correct models and refined models were employed to study

how the material properties vary and how the implant geometry can be optimized under boundary and loading conditions with certain constraints. The consideration of natural root-shaped implants allowed us to model the true biomechanical environment based on biological adaptive growth. Through this procedure, optimized natural root-shaped implants were created for robot milling which will be performed to prepare the root shape for the implant at the implant site. In future research, we will investigate various surface preparation methodologies that will promote bone integration and encourage further stability of these implants. Additionally, we will investigate proper manufacturing methods for such implants.

5 ACKNOWLEDGEMENTS

We would like to thank Harold Clukey and Larry Clukey for their ideas about natural root formed implants and their advisory role in dental implantation.

6 REFERENCES

[1] Nam, J.; Starly, B.; Sun, W.; Darling, A.; Computer-Aided Tissue Engineering, Part I: Overview, Scope and Challenges, J. Biotechnology and Applied Biochemistry, 39(1), 2004, 29-47. DOI: 10.1042/BA20030108

[2] Cook S. D.: A three-dimensional finite element analysis of a porous rooted Co-Cr-Mo alloy dental implant, J. Dent Res, 61, 25-69. DOI: 10.1177/00220345820610010501

[3] Holmgren, E. P.; Kilgren, L. M.; Mante F.; Seckinger, R. J.: Evaluating parameters of osseointegrated dental implants using finite element analysis—a two-dimensional comparative study examining the effects of implant diameter, implant shape, and load direction, Journal of Oral Implantology, 24(2), 1998, 80-88.

[4] Korioth, T. W.; Versluis, A.: Modeling the mechanical behavior of the jaws and their related structures by finite element (FE) analysis, Crit Rev Oral Biol Med, 8, 1997, 90–104. DOI: 10.1177/10454411970080010501

[5] Apicella, A.; Ausiello, P.; Davidson, C. L.; Rengo, S.: 3D-finite element analyses of cusp movements in a human upper premolar, restored with adhesive resin-based composites, J. Biomech, 34, 2001, 1269–1277. DOI: 10.1016/S0021-9290(01)00098-7

[6] Apicella A.; Ausiello, P.; Davidson CL.: Effect of adhesive layer properties on stress distribution in composite restorations—a 3D finite element analysis, Dent Mater, 18, 2002, 295–303. DOI: 10.1016/S0109-5641(01)00042-2

[7] Magne, P.: Efficient 3D finite element analysis of dental restorative procedures using micro-CT data, Dent Mater, 23(5), 2007, 539-548. DOI: 10.1016/j.dental.2006.03.013

[8] Sun, X.; McKenzie, F .D.; Bawab, S.; Li, J.; Yoon, Y.; Huang, J. K.: Automated dental implantation using image-guided robotics: registration results, Int J Comput Assist Radiol Surg., 6(5), 2011, 627-634. DOI: 10.1007/s11548-010-0543-3

[9] Kang, B.; Lang, B.; Lisa, A.L.; Wang, W.: Finite element analysis to determine implant preload, The Journal of Prosthetic Dentistry, 90(6), 2003, 539-546.

[10] Sandu, L.; Topala, F.; Faur, N.: Three dimensional teeth designs generated by NURBS modeling, Eur. Cell Mater, 13(3), 2007, 26.

[11] Fok, S. L.; Romeed, S.A.; Wilson, N.H.: A comparison of 2D and 3D finite element analysis of a restored tooth. J. Oral Rehabil., 33(3), 2006, 209-215. DOI: 10.1111/j.1365-2842.2005.01552.x

[12] MSC.Software Corporation, MSC.PATRAN; http://www.mscsoftware.com/

[13] Baumgartner, A.; Harzheim, L.; Mattheck, C.: SKO (soft kill option): the biological way to find an optimum structure topology, International Journal of Fatigue, 14(6), 1992, 387-393. DOI: 10.1016/0142-1123(92)90226-3

[14] Devlin, H.; Fok, A.; Shi, L.; Li, H.; Ucer, C.: Shape Optimization of Dental Implants, Int J Oral Maxillofac Implants. 2007; 22 (6):911-20.

[15] Li, Q.; Li, W.; Lin, D.; Swain M.: Dental implant induced bone remodeling and associated algorithms, Journal of Mech. Behav. Biomed Mater., 2009 Oct: 2(5), 2008, 410-32.

[16] Cervera, E.; Trevelyan, J.: Evolutionary structural optimization based on boundary representation of NURBS. Part1: 3D algorithms, Computers and Structures, 83, 1917-1929.

[17] Anon.; ABAQUS/Standard User's Manual, Version 6.8 ABAQUS Inc., Providence, RI, 2008. DOI: 10.1016/j.compstruc.2005.02.017